Carbonate reservoirs characterization with seismic phase components attributes from the time-time transform via Variational Auto-Encoder

Pedro Silvany (Petrobras), Marcilio Matos (SISMO), Marcos Machado (Petrobras), Renata Giacomel (Petrobras)

Abstract

Lateral impedance variations associated with thin beds, fluid saturation, and other phenomena can be detected when specific phase components are isolated. However, accurate, continuous phase measurements of a seismic wavelet are more limited in estimating at a given voxel. Multiple means exist to decompose a trace and obtain the phase components. One way is through phase decomposition, which decomposes the seismic amplitude volume into different phase components. We showed that the Time-Time transform provides an alternative means to construct phase components of the seismic amplitude volume. Moreover, we propose a methodology to show the contribution of the Time-Time transform to achieve carbonate geological seismic features detection enhancement by applying a deep Variational Autoencoder in multi-azimuthal seismic data. So, we consider as input multi-channel phase attributes calculated by each azimuth. We also compare the results with those obtained by applying the methodology using the Continuous Wavelet Transform attributes and conventional pre-stack azimuthal seismic data. Finally, we use Gaussian Mixture Models for clustering and obtain probability density functions. This strategy is applied to a Brazilian pre-salt reservoir, showing the Time-Time transform contribution to accurately recognizing carbonate architectural elements such as carbonate mounds.

Introduction

The studies of geological features' automatic classification in seismic data have been the subject of several scientific publications (Dumay & Fournier, 1988; Fournier & Derain, 1995; Johann et al., 2001; Cunha, 2013). The approaches are based on statistical techniques that represent waveform patterns using the vector information from the post-stacked trace (Matos et al., 2010). Furthermore, complementary, joint analyses with seismic attributes, such as time-frequency domain analysis, can be performed to extract characteristics of the seismic signal (Matos et al., 2007) and to enhance the recognition of small-scale structural and stratigraphic heterogeneities in carbonate reservoir environments (Silvany et al., 2021, 2022).

Spectral analysis has been applied to detect bright spots in the presence of thin beds (Cichostępski et al., 2019; Qi et al., 2020). In addition, the complex trace analysis (Taner et al., 1979), which can be viewed as a composition of the envelope amplitude and phase information, also helps to identify small-scale structural and stratigraphic heterogeneities by detecting subtle magnitude (Bulhões & Amorim, 2005) and phase discontinuities due to lateral impedance variations associated with thin beds, fluid saturation, and other phenomena.

By interpreting the Time-time Transform (Pinnegar & Mansinha, 2003) as a kind of local wavelet seismic trace decomposition that, after properly stacked, reconstructs the seismic trace, Matos and Marfurt (2022) showed how to estimate more accurately the local or instantaneous, phase, and use it to decompose the trace into different phase components. They also showed that the TT-transform creates a redundant 2D image from a 1D vector that carries important signal features for pattern recognition.

Recently, (Silvany et al., 2019) showed how to combine deep autoencoders with clustering algorithms to extract seismic facies in multi-azimuth pre-stack seismic data. The Deep Convolutional Autoencoder (DCAE) is used to learn efficient data encodings, reducing the data dimensionality. The latent features generated by the DCAE encoder are used as input to the K-means algorithm.

In this paper, we extend the methodology by applying Variational Autoencoders (VAE) algorithms considering the possibility of jointly using different types of input data, such as Time-Time transform gathers, arranged as different input channels. The VAE algorithm is an unsupervised generative model that also learns efficient data encodings from the seismic data as input (Kingma et al., 2013). Furthermore, unlike an autoencoder (AE) algorithm, the VAE forces the latent variables codes to become normally distributed, making the latent space more continuous and less sparse (Higgins et al., 2021), which brings coded interpretations benefits (Li et al., 2021). Then, a Gaussian Mixture Model (GMM) is applied to fit the data distributions and obtain probability density functions.

This methodology was applied in a pre-salt reservoir from Santo's basin, Southeast Brazilian margin. We compare the Time-Time transform coding results with those obtained by applying the methodology using the Continuous Wavelet Transform (CWT) and conventional pre-stack seismic data. This strategy shows the Time-Time transform contribution to recognizing carbonate architectural elements such as carbonate mounds reservoirs accurately.

Geological Context

The reservoir rocks correspond to a Meso-Neo Aptian age (117-112 Ma) carbonate platform, seated at the culmination of a series of rotated NE-SW and NW-SE oriented faulted blocks that compose the Santos Extern High (SEH) (Silvany et al., 2022) (Figure 1). In this region, the SHE is bounded north and south by a transbacinal NW-SE low-relief transfer zone. This condition led to deposition showing varying petrophysical characteristics, with high to very-high promo-porosities reservoirs identified as carbonatic mounds, contrasting with low energy facies mainly composed of laminites and spherulites.

The low-energy sedimentary facies are dominantly represented by: carbonaceous-siliciclastic mudstone, peloid laminate with a crenulate structure, and dolomite-calcite crust laminate. The Genesis of these fine-grained sediments is related to physical (sedimentation), bio-induced (microbial), and chemical (crust precipitation) processes. To a lesser extent, there are shallow water facies, formed during the decrease of the lake level and footwall uplift, that correspond to incipient microbial shrubs to spherulites (in situ deposits), passing laterally to ooidal to intraclastic grainstones in a context of relatively high energy formed by the action of waves. Also, it occurs in hydrothermal environments with travertine production with anhedral shrubs, indicative of chemical precipitation. Silica cementation occurs mainly as post-depositional diagenesis (Silvany et al., 2022).
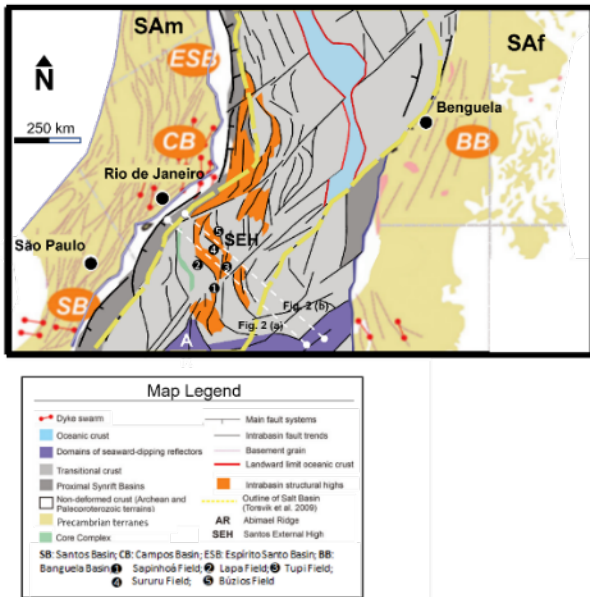

Figure 1 – South America (SAM) and Africa (SAf) shown in a South Atlantic plate reconstruction to 117 Ma. Note the intra-basin architecture, with northern compartments defined by sigmoidal intra-basin fault trends that separate structural lows from structural highs. This region coincides with the area occupied by the Aptian Salt basins of the Central Atlantic. (Modified from Heine et al., 2013, and Araujo et al., 2022).

Data and Method

The Time-Time transform provides an alternative method to estimate local wavelet components of the seismic amplitude volume. Indeed, it transforms a seismic trace with n samples into a pseudo time gather, or an image, with nxn samples, that after stacked reconstructs the trace (Matos and Marfurt, 2022).

In fact, the TT-transform is the last step of the inverse S-transform smartly rewritten by Pinnegar and Mansinha (2003) to operate by this way, that can be attested by considering the S-transform (Stockwell et al., 1996) of a seismic signal, $h(t)$, as a set of localized time-frequency complex functions:

$$S(t,f) = \int_{-\infty}^{\infty} h(\tau) \frac{|f|}{\sqrt{2\pi}} e^{-\frac{f^2(t-\tau)^2}{2}} e^{-j2\pi f\tau}\, d\tau. \tag{1}$$

and its inverse S-transform that reconstructs the original data as

$$h(\iota) = \int_{-\infty}^{\infty}\left\{\int_{-\infty}^{\infty} S(\iota,f)\,d\iota\right\} e^{j2\pi ft}\, df. \tag{2}$$

instead of the original reconstruction property:

$$h(t) = \int_{-\infty}^{\infty}\left\{\int_{-\infty}^{\infty} S(t,f)\,dt\right\} e^{j2\pi ft}\, df. \tag{3}$$

Which shows that the integration of $S(t,f)$ given by equation (1) along the time (, or depth) axis gives the Fourier transform of the input signal.

Therefore, inspired by the reconstruction property the short-time Fourier transform (STFT), Pinnegar and Mansinha (2003) noted that the inverse S-transform can also be evaluated by changing the order of the double integration variables and they defined that the inner integral in equation 2 as the TT-transform, which is a two-dimensional time-to-time representation of the input signal:

$$TT(t,\tau) = \int_{-\infty}^{\infty} S(t,f)e^{j2\pi f\tau}\, df. \tag{4}$$

By this way, the TT-transform is an invertible time-time two-dimensional representation of the seismic data:

$$\int_{-\infty}^{\infty} TT(t,\tau)\,dt - h(\tau) \tag{5}$$

Figure 2 shows the S-transform of a synthetic seismic trace and its corresponding TT-transform. Note that the seismic trace can be perfectly reconstructed by stacking the TT-transform columns.
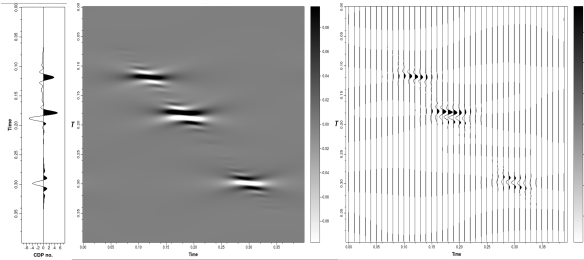
Figure 2 - Synthetic trace and its Time-time transform as an image and as wiggles (decimated).

On other hand, frequency-gathers considered in this paper are the CWT Voices. The CWT Voices are used to create a higher resolution trace and the phase discontinuities to detect small scale structural and stratigraphic heterogeneities. The Continuous Wavelet Transform (CWT) can be interpreted as the cross-correlation between a signal, $f(t)$, and a family of wavelet functions, $\psi_s(t)$. The wavelet family is built by dilating a narrow bandwidth basis function, or "mother wavelet" by a suite of scales, s. By properly dilating and compressing a mother wavelet we can analyze both broad and narrow band signals.

$$WT[f(u,s)] = \int_{-\infty}^{+\infty} f(t) \frac{1}{\sqrt{s}} \psi^*\left(\frac{t-u}{s}\right) dt \qquad (6)$$

$$= f(u) * \overline{\psi_s}(u),$$

Where

$$\overline{\psi_s}(t) = \frac{1}{\sqrt{s}} \psi^*\left(-\frac{t}{s}\right). \qquad (7)$$

Goupillaud et al. (1984) showed that the CWT preserves the signal energy and is invertible, such that the signal can be reconstructed from the CWT coefficients as a convolution along the scales plus an integration along time,

$$f(t) = \frac{2}{C_\psi} \mathcal{R}e \int_0^{+\infty} \int_{-\infty}^{+\infty} CWTf(u,s)\psi_s(t-u)\,du\frac{ds}{s^2} \quad (8)$$

$$= \frac{2}{C_\psi} \mathcal{R}e \int_0^{+\infty} [CWTf(.,s) * \psi_s(t)]\frac{ds}{s^2},$$

(4)
where the constant C_ψ is given by

$$C_\psi = \int_0^{+\infty} \frac{|\Psi(\omega)|^2}{\omega} d\omega \qquad (9)$$

By choosing symmetrical wavelets, in fact complex conjugates wavelets, the CWT cross-correlation operation, can be re-written as a convolution, as shown in equation (1). The CWT can also be interpreted as a bank of pass-band filters, and that the CWT is a joint time-frequency technique.

Inspired by the sound recorded on a tape, Goupillaud et al., (1984), evaluated the CWT using logarithmic frequency scales in voices per octaves, and called as

Voice Transform. Geophysicists would prefer to interpret the CWT inverse transform (equation 4) as a stack of the frequency gathers, i.e., CWT Voices, evaluated form the CWT transform coefficients: $CWTf(.,s) * \psi_s(t)$. Figure 3 shows how we compute the CWT Voices, as frequency gathers, of a Brazilian pre-salt reservoir seismic trace in depth.
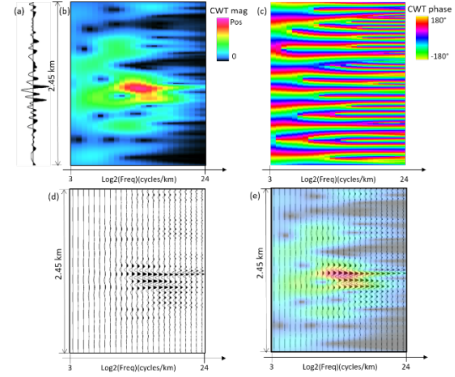

Figure 3 - (a) Seismic trace in depth and its (b) CWT magnitude and (c) phase coefficients, evaluated at 8 voices per octave between 3 and 24 cycles/km. The first step of the inverse CWT is the (d) CWT Voices computation. (e) By corendering CWT mag and CWT Voices, we can clearly see that where the joint depth-frequency magnitude is high, the amplitude of the voices is also high. This is a nice way to confirm the nonlinearity filtering ability of the CWT.

We can assume that the input variables for the deep learning model are a set of matrices {Xi, i=1...N}, in the space, where N1 is the number of time samples and N2 is the number of trances sample (e.g., offsets). To identify the facies, we can treat each matrix Xi as a vector and apply a clustering method over this set of vectors. Clustering means to aggregate the points (vectors) in a number k of collections according to certain similarities. In this paper, we consider the Gaussian Mixture Model (GMM) as a clustering algorithm. The input data are the pre-stack seismic data, the Time-Time transform and CWT Voices attributes both calculated in the post-stack seismic data considering each azimuth.

The space **X** has the dimension of all possible gray images. However, the actual gathers images used are only a small subset of **X**. Work with a high dimension space involves problems known as "curse of dimensionality" (Bellman, 1961). So, assuming that the real gathers images form a manifold embedded in **X**, we will first transform the data with a nonlinear mapping f_θ: **X** → **Z**, where θ are learnable parameters and **Z** is the latent feature space. The dimensionality of **Z** is smaller than the **X**. The set of transformed points {z_i} will be the input to the clustering algorithm. Thus, the method has two steps: (1) the f_θ building and (2) the clustering method application.

To parametrize the function f_θ, it will be used an Auto-Encoding Variational Bayes (AEVB) approach, which a Stochastic Gradient Variational Bayes (SGVB) estimator

to approximate a posterior inference and generate a continuous latent space (Kingma et al., 2013, Doersch, 2016). The process consists of generated a prior distribution $P_\theta * (Z)$ and a value X_i from some prior conditional distribution $P_\theta * (X|Z)$. We assume that the prior and likelihood come from parametric families of distributions $P_\theta * (Z)$ and $P_\theta * (X|Z)$, and that their PDFs are differentiable almost everywhere (Kingma et al., 2013).

The variational Autoencoder architecture is composed by two subnets (Figure 4). The encoder will refer to the probabilistic recognition model $f_\varphi(z|x)$, since given a datapoint X_i it produces a distribution (e.g. a Gaussian) over the possible values of the code Z_i from which the datapoint X_i could have been generated. The encoder subnet is composed by a sequence of convolutional and max pooling layers that is applied over the input as a convolution, which permits to identify patterns in the input image in a way that is invariant with translation. The max pooling layer down samples the input. The encoded distributions are chosen to be normal so that the encoder can be trained to return the mean (Z_{mean}) and the covariance (Z_{dev}) matrix that describe these Gaussians and deviation, which are used to obtain the latent feature $Z = Z_{mean} + Z_{dev}$ for each input X_i (Figure 4).
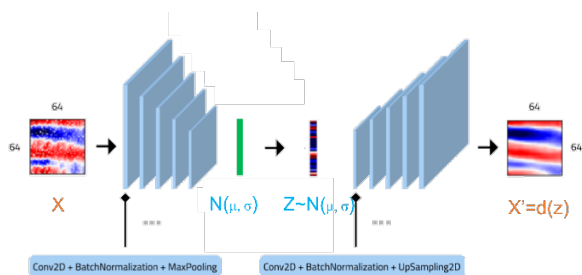

Figure 4 The structure of VAE.

On other hand, the decoder will refer to a probabilistic reconstruction model $f_\theta(x|z)$, since given a code Z_i it produces a distribution over the possible corresponding values of X_i, as similar as possible to the original seismic input. The decoder subnet implements an inverted pyramid: it is composed by a sequence of upsampling and convolution layers. Upsampling layer typically doubles the size of the image, assigning to the output pixel the nearest pixel of the input.

The training of the VAE does not depend on labelled data, it is an unsupervised learning method. The learning is done by minimizing the evidence lower bound (ELBO) objective function (equation 1) (Kingma et al., 2013). The ELBO considers two terms: the first term measured the differences between the posterior and prior gaussian distributions using Kulback-Leibler divergence (KL). This term regularizes the organization of the latent space by making the distributions returned by the encoder $f_\varphi(z|x)$ as close as possible to a standard normal distribution $p_\theta(z)$. The second term measure the reconstruction error for an input X_i, where an encoding Z is sampled from $f_\varphi(z|x_i)$,

then the probability density of a perfect reconstruction is given by $p_\theta(x_i|z)$.

$$\mathcal{L}(\theta, \phi; x) = -DKL(q_\phi(z|x)||p_\theta(z)) + Ez{\sim}q_\phi[\log p_\theta(x|z)] \text{ (eq. 1)}$$

Pre-Salt Reservoir Case Study

The project database comprises three conventional non-dedicated narrow-azimuth seismic surveys with sail-lines heads of N90o, N123o, and N158o, respectively. An opportunity for jointly processing these three seismic volumes was identified, which delivered the pre-stacked multi-azimuthal data.

In this paper, we collected the pre-stack CDP gathers, the Time-Time transform, and CWT Voices frequency gathers from the three available azimuths (N90o, N123o, and N158o) to extract the deep codes **Z**. The chosen interval to select the data comprised the top and base of BVE formation and 25 traces according to the input (offsets or frequency traces). The feature space is generated as a vector space with 32 components (with a dimensionality reduction from 625 to 32). Figure 5 shows (a) eight examples of panels extracted from the Time-Time transform gathers, (b) depth features **Z** encoded by the VAE, and (c) reconstructed images for Azimuth N90o.
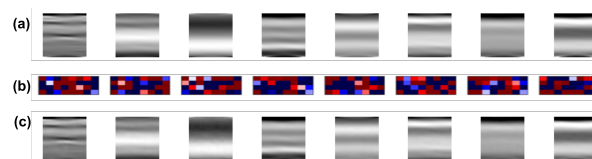

Figure 5 (a) Eight examples of a Time-Time transform gathers panels extracted for Azimuth N90o; (b) Eight examples of deep features **Z** encoded by VAE for Azimuth N90o; (c) Eight examples of reconstructed images for Azimuth N90o.

Figures 6 (a), (b), (c), and (d) show the structural map, the obtained seismic facies with VAE applied in the pre-stack CDP gathers considering azimuths N90o, N123o and N158o, Time-Time frequency gathers, and all input jointly, respectively. One possible interpretation for these maps associates the purple and pink colors regions with the mound facies corresponding to carbonatic growths near the main syn-rift faults and basement highs structures, showing restricted areal distribution and chaotic seismic facies in full-stack amplitude migrated seismic sections. The facies in orange and yellow are related to low-energy facies, which despite their good porosities, present very low permeabilities. The facies in dark and light green are associated with non-reservoir areas (clay deposits).

The Seismic facies obtained using VAE+GMM by considering just the Time-Time transform gathers as input (Figure 6c) show facies with a more continuous and higher resolution if compared with those obtained by the azimuthal pre-stack gathers strategy (Figure 6b). Also, recognizing the architectural elements of deep-water carbonate deposits, specifically to the mound's edges transition to low energy (e.g., laminites) or deep waters

deposits (e.g., magnesium clay), are more consistent with the depositional facies identified by the wells. For instance, well A identified talc-like stevensite layers related to low-energy depositional environments. These minerals are associated mainly with lacustrine deposits in distal settings, while well B identified higher energy carbonates from the BVE (shrubs, stromatolites) (Figure 6). Figure 7 shows the related input data for each centroid associated with the seismic facies from Figure 6C.
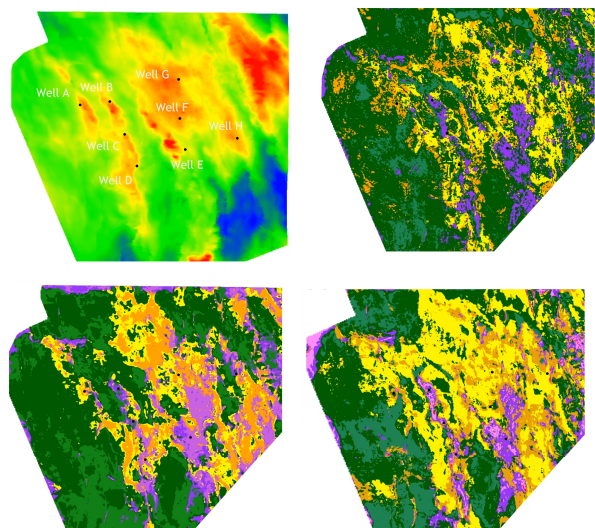

Figure 6 *(a)* Structural map of BVE Formation top; (b) Six facies map obtained by VAE+GMM in three pre-stack CDP gathers (N90o, N123o and N158o); (c) Six facies map obtained by VAE+GMM in three Time-Time transform gathers channels; (d) Six facies map obtained by VAE+GMM in three pre-stack and Time-Time transform gathers.

Nevertheless, the classification of different facies obtained by VAE+GMM applied considering the Time-Time phase gathers, CWT Voices, and pre-stack CDP gathers are more geologically consistent. Also, the results show higher resolution, indicating that, despite the redundancy, using different attributes allowed improved geophysical interpretation. Redundancy plays an important role due to the limited capacity in computational time and architecture learning using deep-learning models. Figure 8 shows the probabilities maps associated with the seismic facies map from Figure 6d.
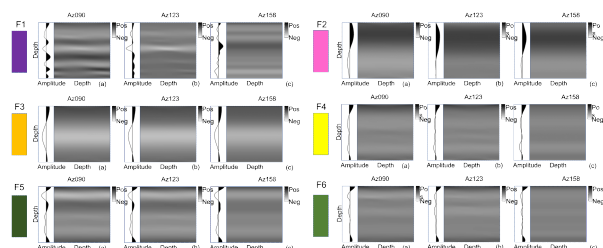

Figure 7 (a) Time-Time transform input gathers for each centroid related with the seismic facies shown in Figure 6c.
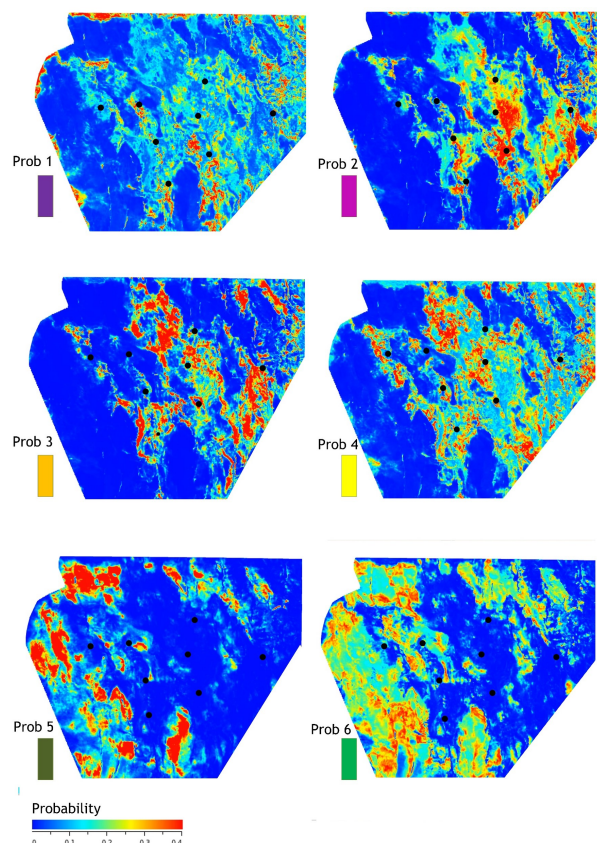

Figure 8 *(a) (b)* Probabilities maps associated with the Mound facies; (c) (d) Probabilities maps associated with low energy facies; (d) (e) Probabilities map associated with lacustrine clay deep water deposits.

Conclusions

Characterizing pre-salt carbonate reservoir seismic facies is a complex process involving uncertainties that shall impact, for instance, non-optimal well locations of the proposed drainage plan. Using VAE in-depth features as input to a clustering method can be obtained seismic facies map using the richness of the pre-stack data. The Time-Time transform gathers improved the recognition of small-scale structural and stratigraphic heterogeneities. Although, the classification of facies using multi-attributes as input is more geologically consistent and shows higher resolution. The redundancy plays an important role due to the limited capacity in computational time and architecture learning using deep-learning models. Furthermore, the results allowed improved geophysical interpretation and brought new insights into the reservoir depositional system.

Acknowledgments

References

Araujo, M. N., Pérez-Gussinyé, M., & Muldashev, I. (2022). Oceanward rift migration during formation of Santos–Benguela ultra-wide rifted margins. *Geological Society, London, Special Publications*, *524*(1), SP524-2021, https://doi.org/10.1144/SP524-2021-123.

Bulhões, E. M., & de Amorin, W. (2005). Princípio da sismocamada elementar e sua aplicação à técnica de volume de amplitudes (TecVa): Anais Ninth International Congress of the Brazilian Geophysical Society. **DOI:** https://doi.org/10.3997 /2214-4609-pdb.160.SBGF276

Cichostępski, K., Dec, J., & Kwietniak, A. (2019). Relative amplitude preservation in high-resolution shallow reflection seismic: a case study from Fore-Sudetic Monocline, Poland. *Acta Geophysica*, *67*, 77-94. DOI: https: //doi.org/10.1007/ s11 600-018-00242-6.

Cunha Filho, C. A., Ruthner, M. P., Gontijo, R. C., & de Almeida, S. H. (2013, August). Statistical Seismic Facies Estimation from Pseudo Impedance Data. In *13th International Congress of the Brazilian Geophysical Society & EXPOGEF, Rio de Janeiro, Brazil, 26–29 August 2013* (pp. 635-638). Society of Exploration Geophysicists and Brazilian Geophysical Society. https://doi.org/10.1190/sbgf2013-131.

Dumay, J., & Fournier, F. (1988). Multivariate statistical analyses applied to seismic facies recognition. *Geophysics*, *53*(9), 1151-1159. https://doi.org/10.1190/1.1442554.

Fournier, F., & Derain, J. F. (1995). A statistical methodology for deriving reservoir properties from seismic data. *Geophysics*, *60*(5), 1437-1450. https://doi.org/10.1190/1.1443878.

Goupillaud, P., Grossmann, A., & Morlet, J. (1984). Cycle-octave and related transforms in seismic signal analysis. *Geoexploration*, *23*(1), 85-102. https://doi.org/10.1016/0016-7142(84)90025-5.

Heine, C., Zoethout, J., & Müller, R. D. (2013). Kinematics of the South Atlantic rift. 757 *Solid Earth*, *4*(2), 215-253, https://doi.org/10.5194/se-4-215-2013.

Higgins, I., Chang, L., Langston, V., Hassabis, D., Summerfield, C., Tsao, D., & Botvinick, M. (2021). Unsupervised deep learning identifies semantic disentanglement in single inferotemporal face patch neurons. *Nature communications*, *12*(1), 6456. DOI: https://doi.org/10.1038/s41467-021-26751-5.

Johann, P., de Castro, D. D., & Barroso, A. S. (2001, March). Reservoir geophysics: Seismic pattern recognition applied to ultra-deepwater oilfield in Campos basin, offshore Brazil. In *SPE Latin American and Caribbean Petroleum Engineering Conference*. OnePetro. https://doi.org/10.2118/69483-MS.

Kingma, D. P., & Welling, M. (2013). Auto-encoding variational bayes. *arXiv preprint arXiv:1312.6114*. DOI: https://doi.org/10.48550/arXiv.1312.6114.

Li, Y., Wang, C., Tian, Y., & Wang, S. (2021). Parameter-shared variational auto-encoding adversarial network for desert seismic data denoising in Northwest China. *Journal of Applied Geophysics*, *193*, 104428. DOI: https://doi.org/10.1016/j.jappgeo.2021.104428.

Matos, M. C., Osorio, P. L., & Johann, P. R. (2007). Unsupervised seismic facies analysis using wavelet transform and self-organizing maps. *Geophysics*, *72*(1), P9-P21. http://dx.doi.org/10.1190/1.2392789

Matos, M. C. D., Marfurt, K. J., & Johann, P. R. (2010). Seismic interpretation of self-organizing maps using 2D color displays. *Revista Brasileira de Geofísica*, *28*, 631-642. http://dx.doi.org/10.1590/S0102-261X2010000400008

Matos, M., & Marfurt, K. (2022, June). Seismic Phase Components from the Time-Time Transform. In *83rd EAGE Annual Conference & Exhibition* (Vol. 2022, No. 1, pp. 1-5). EAGE Publications BV. DOI: https://doi.org/10.3997/2214-4609.202210523.

Pinnegar, C. R., & Mansinha, L. (2003). A method of time–time analysis: The TT-transform. *Digital signal processing*, *13*(4), 588-603. DOI: https://doi.org/10.1016/S1051-2004(03)00022-8.

Qi, J., Zhang, B., Lyu, B., & Marfurt, K. (2020). Seismic attribute selection for machine-learning-based facies analysisChoosing the best seismic attributes. *Geophysics*, *85*(2), DOI: O17-O35. https://doi.org/ 10.1190/geo2019-0223.1.

Silvany, P., Machado, M., & de Tarzo, T. (2019, August). Prestack seismic facies prediction via deep convolutional autoencoders: An application to a turbidite reservoir. In *Proceedings of the 16th International Congress of the Brazilian Geophysical Society*.

Silvany, P. H., Machado, M., Matos, M., & Paes, M. (2021, September). Joint multiazimuthal prestack and time-frequency attributes seismic facies prediction via deep learning: An application to a Brazilian presalt reservoir. In *First International Meeting for Applied Geoscience & Energy* (pp. 1480-1484). Society of Exploration Geophysicists. https://doi.org/10.1190/segam2021-3594815.1.

Sales, P. S., Machado, M. D. C., & Bunevich, R. B. (2022, June). Quality Uncertainty Analysis of Travertine Architectural Elements Associated to Lacustrine Carbonate Deposits Via Deep Transfer Learning. In *83rd EAGE Annual Conference & Exhibition* (Vol. 2022, No. 1, pp. 1-5). EAGE Publications BV. DOI: https://doi.org/10.3997/2214-4609.202210883.

Silvany Sales, P. H., de Araujo, M. N. C., Brandão Bunevich, R., & de Almeida, J. C. H. Control of Basin-Scale Accommodation Zones on Syn-Rift Aptian Lacustrine Carbonate Reservoirs. Implications for Reservoir Quality Estimates of Brazilian Pre-Salt. *Implications for Reservoir Quality Estimates of Brazilian Pre-Salt*. DOI: http://dx.doi.org/10.2139/ssrn.4201284.

Taner, M. T., Koehler, F., & Sheriff, R. E. (1979). Complex seismic trace analysis. *Geophysics*, *44*(6), 1041-1063. DOI: https://doi.org/10.1190/1.1440994.